PROCEEDINGS OF

THE COMBUSTION INSTITUTE

VOLUME 32

Part I

Organized by
THE COMBUSTION INSTITUTE

Investigation of subgrid-scale mixing of mixture fraction and temperature in turbulent partially premixed flames

Jian Cai [a], Danhong Wang [a], Chenning Tong [a,*], R.S. Barlow [b], A.N. Karpetis [c]

[a] *Department of Mechanical Engineering, Clemson University, Clemson, SC 29634-0921, USA*
[b] *Combustion Research Facility, Sandia National Laboratories, Livermore, CA 94551-0969, USA*
[c] *Department of Aerospace Engineering, Texas A&M Univesity, College Station, TX 77843, USA*

Abstract

The filtered mass density function (FMDF) of mixture fraction and temperature used in large eddy simulation (LES) of turbulent combustion is studied experimentally using line images obtained in turbulent partially premixed methane flames (Sandia flames D and E). Cross-stream filtering is employed to obtain the FMDF and other filtered variables. The mean of the FMDF conditional on the subgrid-scale (SGS) scalar variance at a given location are found to vary from unimodal to bimodal, corresponding to quasi-equilibrium distributed reaction zones and laminar flamelets (including extinguished flamelets), respectively. The conditionally filtered mixture fraction dissipation for small SGS variances has a relatively weak dependence on the mixture fraction, and is not sensitive to temperature for extinguished samples. For large SGS variance the large dissipation is concentrated in the cliffs and increases with decreasing temperature. The conditionally filtered temperature dissipation for small SGS variances is the highest for intermediate temperature. For large SGS variance the dependence is more complex and the pilot gas appears to be playing an important role. The different SGS mixture fraction structures for small and large SGS variances, as reflected by the unimodal and bimodal FMDF, have a strong impact on the small-scale mixing and turbulence–chemistry interaction, as reflected by the results for the conditionally filtered temperature dissipation. The results have implications for understanding and modeling multiple reactive scalar SGS mixing.
© 2009 The Combustion Institute. Published by Elsevier Inc. All rights reserved.

Keywords: Turbulent flames; Large-eddy simulation; Filtered density function; Turbulent mixing

1. Introduction

Turbulent mixing and turbulence–chemistry interaction are key processes in turbulent combustion. Accurate predictions of turbulent flames depend critically on correct modeling of these processes. Large-eddy simulation (LES) has been recognized as a very promising approach to modeling turbulent combustion because mixing by the large, resolved scales is computed. At the same time, the instantaneous distribution of scalar values in each grid volume, the filtered mass density function (FMDF), which depends strongly on the subgrid-scale (SGS) scalar mixing and its

---

* Corresponding author. Fax: +1 864 656 4435.
 E-mail address: ctong@ces.clemson.edu (C. Tong).

interaction with chemistry, must be faithfully represented in order to accurately predict the chemical reaction rate [1,2].

The prevailing understanding of turbulent mixing is largely based on the Kolmogorov–Obukhov–Corrsin turbulence cascade theory, which implies certain universal conditional SGS scalar distributions. However, our recent studies of SGS mixing in both reacting and non-reacting flows showed, for the first time, that at a given location the SGS mixture fraction has qualitatively different distributions and structures, depending on the *instantaneous* SGS scalar variance [3,4]. When the SGS variance is small compared to its mean value, the SGS scalar on average has close-to-Gaussian distributions, similar to the scalar probability density function (PDF) in a fully developed scalar field. The scalar dissipation depends weakly on the SGS scalar, indicating well-mixed SGS scalar fields. Such a SGS scalar structure can result in distributed reaction zones. However, when the SGS variance is large compared to its mean value, the SGS scalar on average has bimodal distributions, indicating highly nonpremixed SGS scalar fields. The conditionally filtered scalar dissipation has a bell-shaped dependence on the scalar, resembling the structure of a counter-flow diffusion flame, which is a model for laminar flamelets[5]. This SGS scalar structure is essentially a ramp–cliff structure (see Ref.[6]), with the rich and lean mixtures forming the ramps and the diffusion layer as the cliff. Therefore, such a scalar structure is likely to result in laminar flamelets. In this paper, the term laminar flamelet is used as a general description of a thin, quasi-laminar reaction–diffusion layer rather than the counter-flow flamelet model. The bimodal SGS distributions are similar to the scalar PDF in the early stages of binary mixing, and are contrary to the general considerations based on Kolmogorov's hypothesis.

Our previous results [4] also suggest that at a given location the SGS flame fluctuates between distributed reaction zones and laminar flamelets, but for reasons different from previous arguments based on scalar dissipation fluctuations resulting from the turbulence cascade. In addition, a significant amount of scalar dissipation rate in the reaction zones, which, to the first-order approximation, is proportional to the heat release, comes from the ramp–cliff structure, highlighting its importance in flames and the need for mixing models to capture the bimodal FMDF to account for the different flame structures.

In this study we investigate the SGS mixing of mixture fraction and temperature. We focus on the effects of the two types of the SGS mixture fraction structures on the scalar dissipation and temperature dissipation. Temperature is arguably the most important reactive scalar and is widely measured in turbulent flames. Its mixing process is expected to be very different from that of the mixture fraction. Therefore, investigations of these dissipation rates are an important step in understanding the SGS mixing of multiple reactive scalars and its interaction with combustion chemistry. The results are also relevant for improving several modeling approaches including the laminar flamelets, the conditional moment closure, and the FMDF approaches.

The filtered mass density function of mixture fraction and temperature is

$$F_{\xi TL}(\hat{\xi}, \hat{T}; \mathbf{x}, t) = \langle \rho(\mathbf{x}, t)\delta(\xi - \hat{\xi})\delta(T - \hat{T})\rangle_{\ell}$$

$$= \int \rho(\mathbf{x}', t)\delta(\xi - \hat{\xi})\delta(T - \hat{T})$$

$$\times G(\mathbf{x} - \mathbf{x}')\,d\mathbf{x}', \quad (1)$$

where ξ, T, $\hat{\xi}$, and $\hat{T}$ are the mixture fraction, temperature, and their sample-space variables, respectively. ρ is the fluid density. The subscripts ℓ and L denote conventional and Favre-filtered variables, respectively. The two most important variables evolving the FMDF are the conditionally filtered scalar dissipation, $\langle \chi | \xi, T \rangle_{\ell} = \langle D\frac{\partial \xi}{\partial x_j}\frac{\partial \xi}{\partial x_j}|\xi, T\rangle_{\ell}$, and the conditionally filtered temperature dissipation, $\langle \chi_{\mathrm{T}} | \xi, T \rangle_{\ell} = \langle D_{\mathrm{T}}\frac{\partial T}{\partial x_j}\frac{\partial T}{\partial x_j}|\xi, T\rangle_{\ell}$.

2. Experimental data

We use experimental data obtained in piloted turbulent partially premixed methane flames with a 1:3 ratio of CH_4 to air by volume (Sandia flames D and E, see Refs.[7–9]). The measurements employed combined line-imaging of Raman scattering, Rayleigh scattering, and laser-induced CO fluorescence. Simultaneous measurements of major species (CO_2, O_2, CO, N_2, CH_4, H_2O, and H_2), mixture fraction (obtained from all major species), temperature, and the radial component of scalar dissipation rate were made. The mixture fraction is calculated using a variation of Bilger's definition, which has been modified by excluding the oxygen terms [7].

The issue of measurement uncertainty was addressed in Ref.[7], which concluded that the accuracies of the measured species mass fractions, temperature, and mixture fraction are sufficient. For example, the measured values of the scalar variance in uniform calibration flows were 10^{-6} in air and 10^{-5} in flat stoichiometric flame products and in jet fluid, respectively.

The length of the imaging line is 6.13 mm with a measurement spacing of 0.2044 mm. The actual measurement resolution is larger (≈ 0.3 mm) due to the blurring effects of the optical system and data processing [10]. The mean scalar dissipation rate for is fully resolved for flame D and is slightly under-resolved for flame E at $x/D = 7.5$ [10]. However, this resolution might still under-resolve

very large dissipation fluctuations, thereby under-estimating the conditionally filtered dissipation rate in cliffs. Our analyses (will be published in a separate paper) show that for this resolution the conditionally filtered dissipation for small SGS variance (computed from the gradient component along the line images) is well resolved using second-order finite differencing. However, for large SGS variance a sixth-order finite difference stencil is needed to resolve the ramp–cliff structure, whose gradient has an average FWHM ranging from 0.5 to 0.75 mm. Therefore, we use sixth-order center differencing to compute the dissipation rates. We also corrected for the noise contribution to the scalar dissipation rate. The method for noise correction and estimation of the scalar dissipation length scales will be published in a separate paper.

Computing the FMDF and SGS variables from experimental data requires spatial filtering of scalar fields. In this work, one-dimensional filtering is employed. While in LES the filtering is generally performed in three dimensions, our previous results have shown that the scalar filtered density function (FDF) obtained with one-dimensional filters is similar to that obtained with two-dimensional filters [3,11], which has been shown to be a very good approximation of three-dimensional filtering, with errors of approximately 5% for the rms resolvable- and subgrid-scale variables [12]. In general, the functional form of the conditionally filtered variables and the filtered (mass) density functions are not sensitive to the filter dimension, a result of the random orientation of the instantaneous flow and flame structure. The main effect of the filter dimension is that the SGS variance value is slightly altered. For a similar level of bimodality for the FDF, the SGS scalar variance is somewhat larger for one-dimensional filters, which are therefore expected to yield similar results as three-dimensional filters. To ensure that the results are relevant to LES the filter sizes Δ employed in this work (3.07 and 4.91 mm) are significantly larger than the dissipative (Corrsin) scales (0.065–0.106 mm [10]), such that the subgrid scales contain sufficient fluctuations, allowing the physics of the SGS mixing and its interaction with chemistry to be related to inertial-range dynamics. Only when the filter size approaches the dissipation scales does the FDF depend more strongly on the filter scale.

In our analyses 6000 line images are used at each measurement location. Due to the limited data size, we employ kernel methods for computing the FMDF and the conditionally filtered dissipation rates. We use a bin width of $\Delta ln\langle \xi''^2 \rangle = 1.3$ to achieve reasonable statistical convergence. Further reduction of the bin size would slightly increase the bimodality of the bimodal conditional SGS scalar. Therefore, the conclusions regarding the bimodal FMDF and the dissipation rates are somewhat conservative.

3. Results and discussions

In this section the results of the measured FMDF and the conditionally filtered dissipation rates are presented. Unlike a PDF and the conditional dissipation, the FMDF and the conditionally filtered dissipation rates are random variables; therefore must be characterized by their statistics. We employ the approach given in Ref. [3]) which computes their conditional averages. We use the Favre-filtered mixture fraction,

$$\langle \xi \rangle_{\rm L} = \langle \rho \xi \rangle_\ell / \langle \rho \rangle_\ell, \qquad (2)$$

and the Favre SGS scalar variance,

$$\langle \xi''^2 \rangle_{\rm L} \equiv \frac{1}{\langle \rho \rangle_\ell} \int F_{\xi L}(\hat{\xi}; \mathbf{x}, t)(\hat{\xi} - \langle \xi \rangle_{\rm L})^2 \, \mathrm{d}\hat{\xi}$$
$$= \langle \rho \xi^2 \rangle_\ell / \langle \rho \rangle_\ell - \langle \xi \rangle_{\rm L}^2 \qquad (3)$$

(also random variables) as conditioning variables, which provide a measure of the unmixedness of the mixture fraction and have proven to be very effective for characterizing FMDF and for relating the FMDF to inertial-range dynamics [3], both important for modeling SGS mixing.

3.1. The conditional mixture fraction-temperature FMDF

The conditional mixture fraction FMDF, $\langle F_{\xi T} | \langle \xi \rangle_{\rm L}, \langle \xi''^2 \rangle_{\rm L} \rangle$, for flame D and E at 7.5 jet diameters downstream of the jet exit ($x/D = 7.5$) is shown in Fig. 1. The filtered mixture fraction, $\langle \xi \rangle_{\rm L}$, is set to the stoichiometric mixture fraction, $\xi_{\rm s}(= 0.35)$, to maximize the probability of the SGS field containing reaction zones. For flame D there is little local extinction at this location and the FMDF for both small and large SGS variance is concentrated not far from the equilibrium values. For small SGS variance, e.g. $\langle \xi''^2 \rangle_{\rm L} \approx 0.0047$ (Fig. 1a), the conditional FMDF is unimodal. The peak of the FMDF (most samples) is near the equilibrium values. Due to the well mixed SGS scalar the SGS reactions are expected to be in the quasi-equilibrium reaction zones regime. For flame E there is some local extinction as reflected by the low temperature but the results are otherwise similar to those for flame D.

As the SGS variance increases, the FMDF becomes bimodal (Fig. 1b and d) with the bimodality stronger for larger SGS variance. The peaks are at $\xi = 0.17$ and 0.62, indicating that the rich and lean mixtures in the SGS field (i.e., a grid cell) are essentially segregated. Furthermore, there is a sharp interface (diffusion-layer) separating the two regions, across which there is a large scalar value jump (also see the discussion on the conditionally filtered scalar dissipation rate below). For flame D although most samples are still far from extinction, the temperature near $\xi = 0.4$ is already lower than that for the small SGS
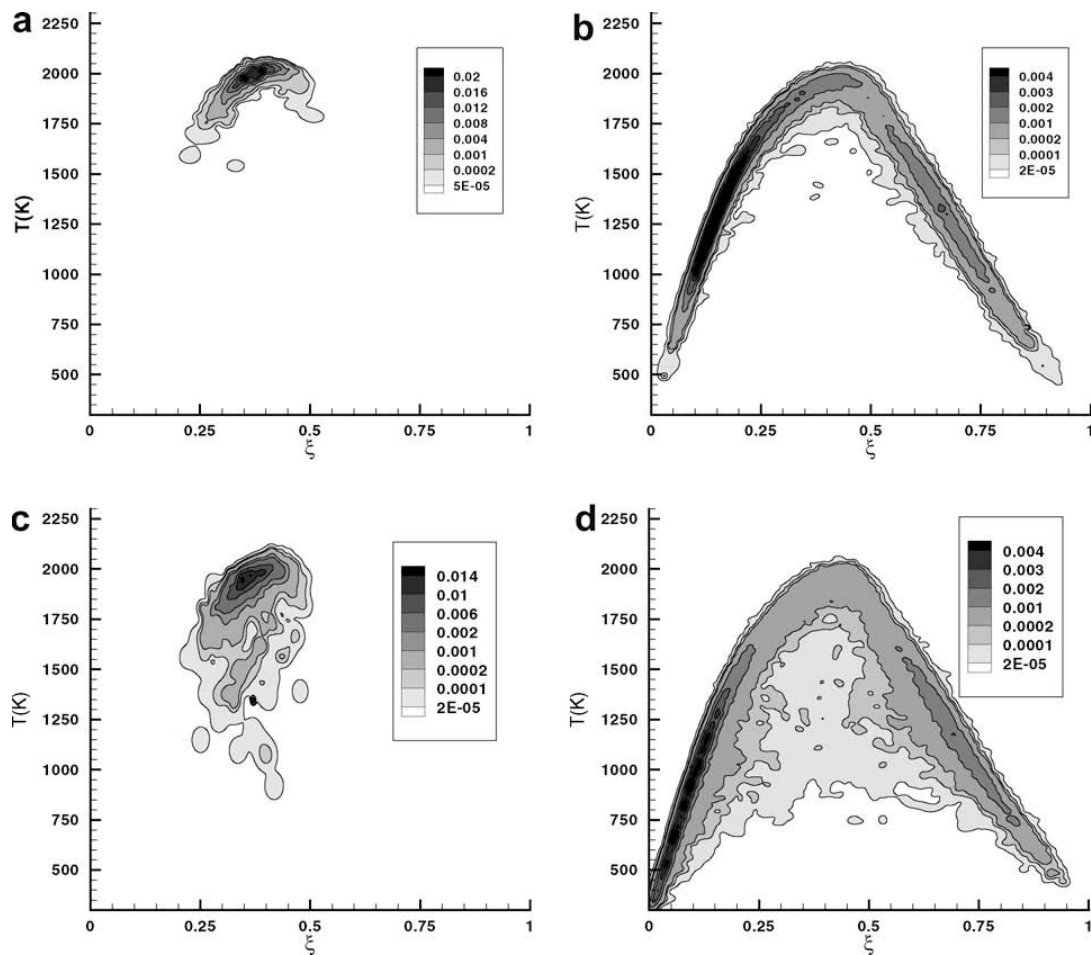
Fig. 1. Conditional FMDF at $x/D = 7.5$. (a) flame D, $\langle \xi''^2 \rangle_L = 0.0013$; (b) flame D, $\langle \xi''^2 \rangle_L = 0.066$; (c) flame E, $\langle \xi''^2 \rangle_L = 0.0011$; (d) flame E, $\langle \xi''^2 \rangle_L = 0.081$.

variance. For a bimodal FMDF the SGS scalar contains two relatively well-mixed mixtures corresponding to the two peaks of the FMDF. The difference between the ξ values of the two mixtures is often greater than the reaction zone width in the ξ space for these methane flames, $\Delta \xi_R (\approx 0.23)$, defined by the lean and rich limits that correspond to 10% of the peak CO oxidation reaction rate in mildly strained laminar flames [13]. Therefore, such a mixture fraction structure will limit the reaction zones in thin diffusion layers, thereby resulting in laminar flamelets. By contrast, for the well-mixed SGS mixture fraction field, the turbulence cascade is likely to dominate and the dissipation-scale scalar fluctuations largely follow the Kolmogorov–Obukhov–Corrsin predictions. Therefore, such a SGS scalar is likely to result in distributed reaction zones. For flame E the FMDF values near equilibrium are lower than for flame D and there is a relatively large probability of local extinction due to the large scalar dissipation rate with temperature as low as 1000 K. These results are consistent with the mixture fraction FMDF [4].

At $x/D = 15$, there are more extinguished samples for both flame D and E (Fig. S1). For small

SGS variance, the FMDF shape is similar to that at $x/D = 7.5$. For large SGS variance, the FMDF peak on the rich side is broader due to the increased temperature variations, therefore the peak value is lower. The amount of local extinction in flame E (Fig. S2) is approximately five times that in flame D. At $x/D = 30$, the probability of local extinction is approximately 2–3 times lower than at $x/D = 15$ because the scalar dissipation is reduced as the flames evolve downstream.

The filter scale is an important parameter in LES and it is important to understand how the FMDF varies with it. Our previous results have shown that increasing the filter scale does not alter the shape of the FMDF. The results in the present study (not shown) are consistent with this finding.

3.2. The conditionally filtered scalar dissipation

The conditionally filtered scalar dissipation, $\langle \langle \chi | \xi, T \rangle_\ell | \langle \xi \rangle_L, \langle \xi''^2 \rangle_L \rangle$, for the same conditions as Fig. 1 is shown in Fig. 2. Here we have limited the domains of the conditioning variables ξ and T to those of the corresponding FMDF shown in Fig. 1. Similar to the FMDF, $\langle \chi | \xi, T \rangle_\ell$ also has qualitatively different functional forms for
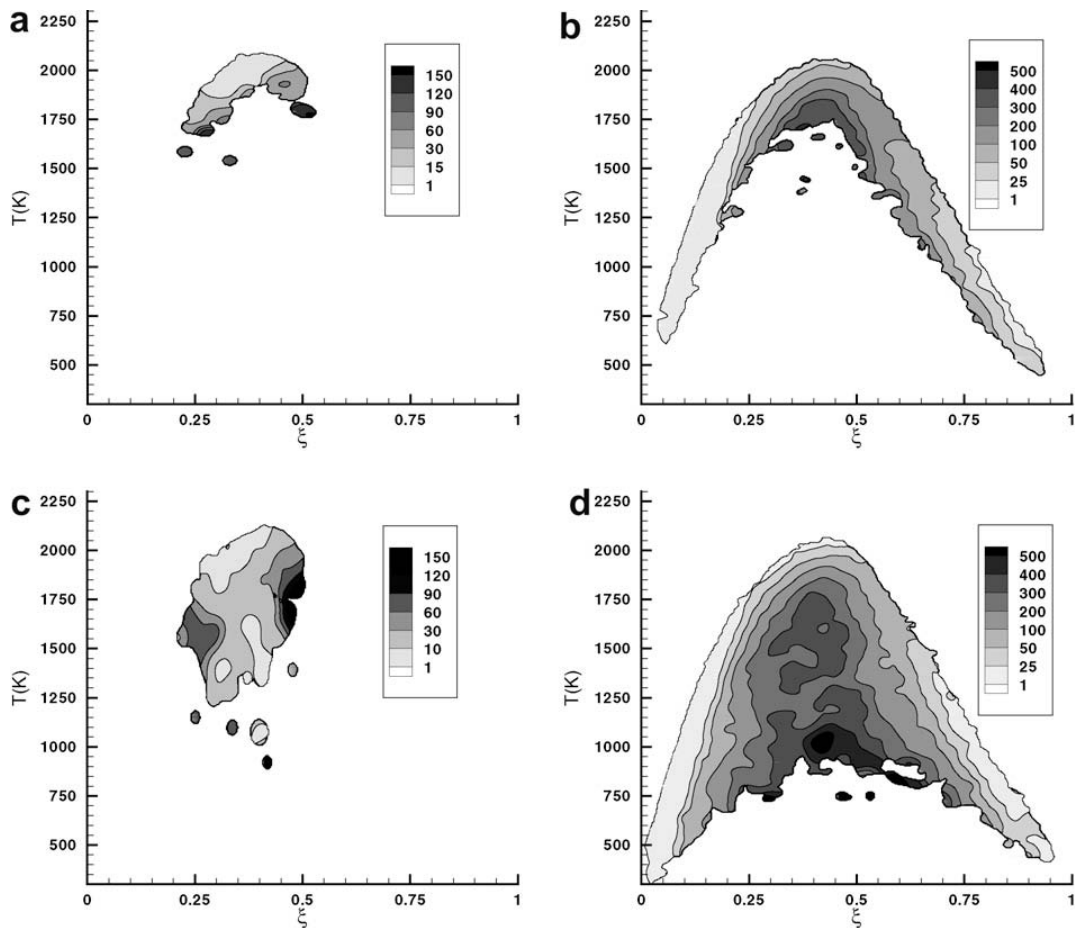
Fig. 2. Conditionally filtered mixture fraction dissipation. Conditions same as in Fig. 1.

small and large SGS variance. At $x/D = 7.5$, flame D (Fig. 2a and b) has little local extinction. For small $\langle \xi''^2 \rangle_L$ it has a relatively weak dependence on ξ, consistent with the conditional FMDF being unimodal. However, higher dissipation rate generally corresponds to lower temperature. The observed temperature–scalar-dissipation correlation for a fixed mixture fraction is consistent with the expectation that in quasi-equilibrium distributed reaction zones the temperature decreases as the scalar dissipation increases [14].

In flame E the samples close to equilibrium have a similar dependence on ξ and T (Fig. 2c). However, flame E already has a significant amount of local extinction but the scalar dissipation near the stoichiometric mixture fraction at lower temperature (1250–1750 K) does not depend strongly on temperature.

For large $\langle \xi''^2 \rangle_L$, the conditionally filtered dissipation in flame D (Fig. 2b) is generally large near $\xi = 0.4$–0.45, where the maximum gradient in the ramp–cliff structure is located[4]. The maximum value increasing with the SGS variance value (not shown). Near the equilibrium values the scalar dissipation is generally larger for lower temperature, consistent with the characteristics of strained laminar flamelets. Again, at $x/D = 7.5$,

flame D has little local extinction; therefore the conditional dissipation does not extend to very low temperatures. For flame E, the samples close to equilibrium are similar to those in flame D. Further away from equilibrium at lower temperatures the dissipation rate is larger and there is a significant amount of local extinction. The highest value (one component) of approximately 700 s^{-1} observed in some images (not shown), which well exceeds the extinction dissipation rate for a steady laminar flamelets, occurs at very low temperature (approximately 750 K). Considering the reduced diffusivity at these temperatures, the high dissipation rate is likely caused by very high strain rates. Because the SGS scalar contains ramp–cliff structure, these samples are most likely extinguished laminar flamelets.

At $x/D = 15$ flame D (Figs. S3a and S3b) has a larger number of extinguished samples with very low temperatures (<1300 K) and the dissipation is qualitatively similar to those for flame E at $x/D = 7.5$. When the SGS variance is small, the dissipation rate increases with decreasing temperature for the burning samples. The dependence is insensitive to the ξ values, similar to the results shown in Fig. 2c. For the extinguished samples the peak conditional dissipation rate is

approximately 150 s^{-1}, below the extinction rate for steady laminar flamelets ($\approx$ 400 s^{-1})[15]. Therefore these might be samples extinguished upstream. As they are advected downstream to the measurement location the scalar dissipation rate has reduced but they have not yet mixed with high temperature parcels to reignite. Therefore, their temperatures remain low. The results for Flame E show a similar trend (Fig. S4a). Previous DNS of nonpremixed combustion in isotropic turbulence [16] also showed a similar evolution process.

For large SGS variance both flame D and E (Figs. S3a and S4a) have extinguished samples, with the latter having approximately five times more but the scalar dissipation results are similar to those at $x/D = 7.5$. The maximum conditionally filtered dissipation rate is reduced to 500 s^{-1} for both flames.

At $x/D = 30$ (Figs. S3c-d and S4c-d), there is a significant amount of reignition and the probability for extinguished samples is reduced. For small SGS variance, the dependence of the dissipation on ξ is weaker compared to $x/D = 7.5$ and 15. For large SGS variance the maximum conditionally filtered dissipation rate remains approximately 500 s^{-1} for both flames. However, the probability of occurrence for the large variance is smaller compared to the upstream locations, consistent with the reignition and the reduced degree of local extinction.

3.3. The conditionally filtered temperature dissipation

The above results indicate that the different structures of the SGS mixture fraction fields for small and large SGS variances result in different conditionally filtered scalar dissipation. Through interaction with combustion chemistry, the SGS mixture fraction fields will result in qualitatively different temperature dissipation structure. We now examine the conditionally filtered temperature dissipation, which is shown in Fig. 3. In flame D at $x/D = 7.5$ the temperature is close to the equilibrium values for small SGS variance. Near $\xi = 0.45$ the flame reaches the local maximum temperature, leading to the lowest temperature dissipation. Away from $\xi = 0.45$ the temperature dissipation is small near the equilibrium values and increases with decreasing the temperature decreases. There is some similarities between the conditional temperature dissipation and the conditional scalar dissipation samples for the rich and lean mixtures because for these mixtures there exists correlation between ξ and T near the equilibrium curve (positive for $\xi < 0.4$ and negative for $\xi > 0.4$). Therefore, the temperature dissipation increases with the scalar dissipation for these mixture fraction values. In flame E there are some non-burning samples with higher χ_T but the results are otherwise similar to those for flame D.

For large SGS variance, flame D is still close to fully burning. For the samples not far from equilibrium, large temperature dissipation values occur in rich mixtures with ξ values ranging from 0.5 to 0.65, but not in the lean mixtures. This is a result of the strained laminar flamelet structure. For a flamelet far from extinction $T = T(\xi, \chi_s)$ and $\frac{\partial T}{\partial y} = \frac{\partial T}{\partial \xi}\frac{\partial \xi}{\partial y}$, where χ_s is the scalar dissipation rate at the stoichiometric mixture fraction. Because $\frac{\partial T}{\partial \xi}$ is V-shaped with a minimum (zero) near $\xi = 0.45$ and at the same time $\frac{\partial \xi}{\partial y}$ is bell-shaped with its peak value located near $\xi = 0.5$ (Fig. 2b), large values of $\frac{\partial T}{\partial \xi}\frac{\partial \xi}{\partial y}$ and the temperature dissipation occur for ξ values ranging from 0.5 to 0.65. Further away from equilibrium, there are some large χ_T values on both the rich and lean side of the flame. An examination of the line images (Fig. S5a) indicates that the lean sides of the images have the shape of strained laminar flamelets, indicating that the lean sides of the laminar flamelets are nearly fully burning. However, the large χ_T values on the rich sides come from images that contain straight lines in the $\xi - T$ space, running from ξ_s to the rich side, indicating that the samples are being mixed but not burning. At this location a significant portion of the SGS stoichiometric mixture for large SGS variance may be the pilot flame gas, suggesting that the high temperature dissipation values are largely due to the mixing of the pilot gas with the rich mixtures. Because the scalar dissipation rate is high, mixing is much faster than reaction, resulting a mixing line (mixing without reaction). Similar straight mixing lines have been observed in double scalar mixing layers [17]. This observation suggests that each of these laminar flamelets is split by the pilot gas, effectively forming two flamelets, one lean and one rich. It has been suggested [8,18] that the pilot gas has been throughly mixed at $x/D = 7.5$. While on average the amount of pilot gas may be small at this location, the conditional samples for large SGS variance still contain a significant amount because these conditional samples are much less well mixed. In fact nearly pure pilot gas can be found as far as $x/D = 15$ (see the discussions below).

The results for the near equilibrium samples in flame E are similar except that the largest χ_T comes from the mixing of the pilot and the lean mixtures. For the extinguished samples at much lower temperature (<1200 K) the line images in the $\xi - T$ space include ones running from near stoichiometric mixture to both sides as well as straight lines running from the lean side to the rich side of the equilibrium curve, consistent with extinguished laminar flamelets.

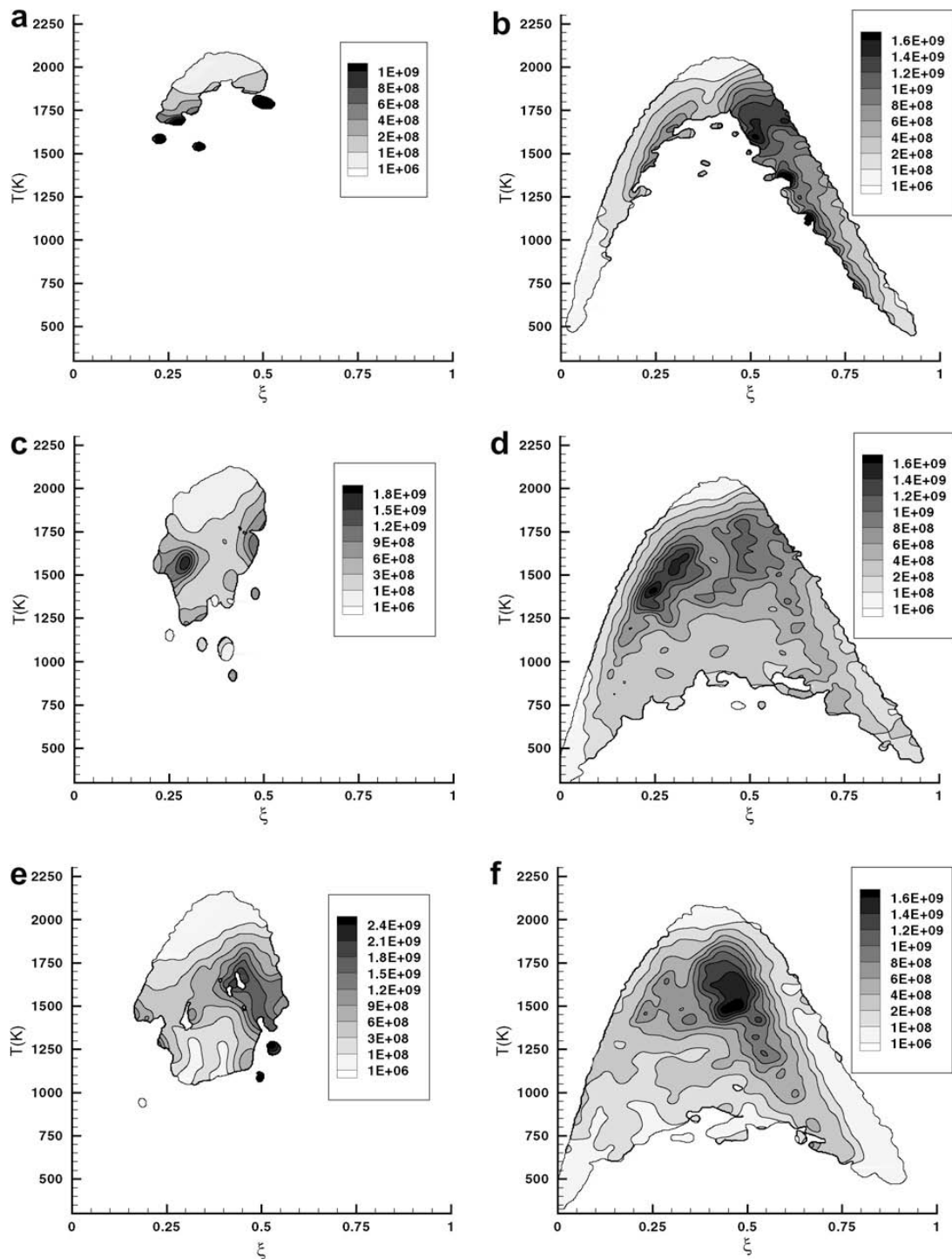At $x/D = 15$ a number of extinction events occur for both small and large SGS variance values.

Fig. 3. Conditionally filtered temperature dissipation. (a–d) Conditions same as in Fig. 1, (e) flame D, $x/D = 15$, $\langle \xi''^2 \rangle_L = 0.0030$, and (f) flame D, $x/D = 15$, $\langle \xi''^2 \rangle_L = 0.069$.

In flame D for small SGS variance the samples close to equilibrium have similar temperature dissipation structures to those at $x/D = 7.5$ with low χ_T near $\xi = 0.45$ (Fig. 3e). The extinguished samples with very low temperatures (<1300 K) generally have small temperature dissipation because the temperature gradient is reduced by mixing. In addition, lower diffusivities resulted from the reduced temperature can also contribute to the lower dissipation rates. The samples with intermediate temperatures (1300–1600 K) have the highest temperature dissipation which is likely a result of mixing between the burning and extinguished samples. The dependence on the mixture fraction is relatively weak compared to samples with higher temperature because T and ξ no longer follow the equilibrium relationship. Therefore, these samples have high χ_T but relatively low χ.

For large SGS variance, χ_T for the burning samples (close to equilibrium) is similar to that at $x/D = 7.5$ with large values near $\xi = 0.55$.

The dissipation is maximum near $\xi = 0.5$ and $T = 1600$ K. The line images going through this region in the $\xi - T$ space (Fig. S5b) show that the lean sides of the images mostly have the shape of strained laminar flamelets. There are a few straight lines, suggesting more intense mixing between the pilot and the air than at $x/D = 7.5$, probably due to the spreading of the turbulence towards the lean side. The rich sides contain more straight lines in the $\xi - T$ space than at $x/D = 7.5$, running from ξ_s to the rich sides, again indicating that these samples are being mixed but not burning. At this location we expect that the proportion of pilot gas at the stoichiometric mixture to be much smaller compared to $x/D = 7.5$, but apparently there is still a sufficient amount to form a mixing line on the rich side. Therefore, the high temperature dissipation is largely due to the rapid mixing of the pilot gas with the rich mixtures. The mixing is faster than the reactions, resulting a mixing line. Again, the results suggest that each of these laminar flamelet is split by the pilot gas to form two flamelets with one on the lean side burning and the one on the rich side extinguished. For the samples at much lower temperature (<1200 K) the line images in the $\xi - T$ space are straight line from the lean to the rich side, consistent with extinguished laminar flamelets. There is no apparent evidence of the pilot separating the lean and rich side. This is probably because the pilot gas is already mixed with the rest of the fluid due to large χ in these flamelets. The results for flame E (Fig. S7a-b) are similar.

At $x/D = 30$ (Figs. S6a and Fig. S7c) for small SGS variance χ_T is low for high temperatures and is higher for intermediate temperatures (1500–1800 K). Due to reignition there are fewer samples with temperature below 1500 K. For large SGS variance (Figs. S6b and Fig. S7d), χ_T has two peaks near $\xi = 0.3$ and 0.5 and $T = 1600$ K although the peak values are smaller. These are again due to mixing of near stoichiometric mixture with lean and rich mixtures. The dissipation rate is approximately the same for both peaks whereas at $x/D = 7.5$ and 15, one peak dominates.

The temperature dissipation results indicate that for small SGS variance, which corresponds to distributed reaction zones, there is temperature mixing in the absence of significant mixture fraction mixing. On the other hand, for large SGS variance, mixture fraction mixing and temperature mixing proceed simultaneously as in laminar flamelets. These qualitatively different properties of SGS mixing must be reflected by mixing models.

4. Conclusions

The filtered mass density function of mixture fraction and temperature and the conditionally fil-

tered mixture fraction and temperature dissipation rates which evolve the FMDF are studied experimentally. Data obtained in turbulent partially premixed flames (Sandia flames D and E) are used to compute SGS statistics conditional on Favre filtered mixture fraction and the Favre SGS scalar variance.

The results show that the FMDF has qualitatively different shapes for small and large SGS variance. For small SGS variance the FMDF is unimodal but for large SGS variance it is bimodal with the two peaks outside of the reaction zone. These FMDF shapes correspond to quasi-equilibrium distributed reaction zones and laminar flamelets (including extinguished flamelets), respectively. Changing the filter scale from 3.07 to 4.91 mm does not alter the shapes of the FMDF.

The conditionally filtered mixture fraction dissipation for small SGS variances is generally consistent with quasi-equilibrium distributed reaction zones with a relatively weak dependence on the mixture fraction. For the extinguished samples it is not very large and is not sensitive to the temperature, suggesting that these may be samples extinguished at some upstream locations. For large SGS variance, the dissipation is large near $\xi = 0.4$, where the maximum gradient in a cliff is located. The dissipation is higher for lower temperatures, consistent with strained laminar flamelets. For the extinguished samples, the measured dissipation rate component exceeds the extinction dissipation rate. The results are consistent with extinguished flamelets.

The conditionally filtered temperature dissipation for small SGS variances has a minimum (close to zero) near the peak temperature at approximately $\xi = 0.45$. Away from this mixture fraction value the dissipation increases. For the extinguished samples with very low temperatures (<1300 K), the dissipation is lower compared to those with intermediate temperatures (1300–1600 K). The latter is due to the mixing between burning and very low temperature samples. Therefore, the mixture fraction is well mixed but temperature is not.

For large SGS variance, the dissipation indicates strained or extinguished laminar flamelets. However, the pilot flame plays an important role. For samples not far from equilibrium, the dissipation is consistent with strained laminar flamelets with the maximum dissipation occurring near $\xi = 0.55$. Further away from equilibrium at moderate temperature (as high as 1700 K) there are dissipation peaks which are probably a result of the rapid mixing between the pilot gas and the lean or rich mixtures, corresponding to extinguished flamelets. There is also evidence that each of these flamelets is split by the pilot gas. At much lower temperature the dissipation is lower because the temperatures of the extinguished flamelets are lower, corresponding to lower dissipation.

We note that there have previous efforts to infer χ from χ_T experimentally. The present work shows that although there are some similarities between the two dissipation rates, in the reaction zone they are qualitatively different with the latter being dependent on both the turbulence and turbulence–chemistry interaction. Therefore, the mixture fraction structure near the stoichiometric mixture fraction, arguably the most important part of the structure, cannot be inferred from the temperature dissipation. The implications are that the two variables are related to different processes and that they cannot be modeled the same way.

The results in the present study show that the different mixture fraction structures for small and large SGS variances as reflected by the unimodal and bimodal FMDF have a strong impact on the small-scale mixing as reflected by the results for conditionally filtered mixture fraction dissipation and turbulence–chemistry interaction as reflected by the results for the conditionally filtered temperature dissipation. The results have implications for understanding multiple reactive scalar SGS mixing and for modeling SGS mixing.

Acknowledgments

Appendix A. Supplementary data

Supplementary data associated with this article can be found, in the online version, at doi:10.1016/j.proci.2008.05.026.

References

[1] S.B. Pope, *Proceedings of the 23rd Symposium (International) on Combustion*, 1990, pp. 591–612.
[2] P.J. Colucci, F.A. Jaberi, P. Givi, S.B. Pope, *Phys. Fluids* 10 (1998) 499–515.
[3] C. Tong, *Phys. Fluids* 13 (2001) 2923–2937.
[4] D. Wang, C. Tong, R.S. Barlow, A.N. Karpetis, *Proc. Combust. Inst.* 31 (2007) 1533–1541.
[5] N. Peters, *Prog. Eng. Combust. Sci.* 10 (1984) 319–339.
[6] C. Tong, Z. Warhaft, *Phys. Fluids* 6 (1994) 2165–2176.
[7] R.S. Barlow, A.N. Karpetis, *Flow Turbul. Combust.* 72 (2004) 427–448.
[8] A.N. Karpetis, R.S. Barlow, *Proc. Combust. Inst.* 30 (2005) 665–672.
[9] R.S. Barlow, A.N. Karpetis, *Proc. Combust. Inst.* 30 (2005) 673–680.
[10] G. Wang, A.N. Karpetis, R.S. Barlow, *Combust. Flame* 148 (2007) 62–75.
[11] D. Wang, C. Tong, *Phys. Fluids* 14 (2002) 2170–2185.
[12] C. Tong, J.C. Wyngaard, S. Khanna, J.G. Brasseur, *J. Atmos. Sci.* 55 (1998) 3114–3126.
[13] J.H. Frank, S.A. Kaiser, M.B. Long, *Proc. Combust. Inst.* 29 (2002) 2687–2694.
[14] R.W. Bilger, *Proceedings of the Twenty-Second Symposium (International) on Combustion*, 1988, pp. 475–488.
[15] A.N. Karpetis, R.S. Barlow, *Proc. Combust. Inst.* 29 (2002) 1929–1936.
[16] P. Sripakagorn, S. Mitarai, G. Kosaly, H. Pitsch, *J. Fluid Mech.* 518 (2004) 231–259.
[17] S. Mitarai, S.M. de Bruyn Kops, C.M. Cha, *Combust. Flame* 149 (2007) 392–408.
[18] H. Pitsch, H. Steiner, *Proc. Combust. Inst.*, 2000, pp. 41–49.